REPRINTED FROM PROCEEDINGS OF THE INTERNATIONAL CONFERENCE ON LASERS '87, DECEMBER 7–11, 1987

INTENSE PICOSECOND LIGHT GENERATION BY AMPLIFIED SPONTANEOUS EMISSION

P. Sperber, W. Spangler, B. Meier, and A. Penzkofer
Naturwissenschaftliche Fakultät II - Physik,
Universität Regensburg, D-8400 Regensburg, Fed.Rep.Germany

The picosecond pulse generation in longitudinally pumped dye laser generators and amplifiers is studied. Frequency tunable pulses between 720 nm and 940 nm are generated with a picosecond ruby pump source. Energy conversion efficiences of approximately ten percent are obtained. Besides the amplification of spontaneous emission, the seeding pulse amplification of picosecond light continua is discussed. The simultaneous occurrance of resonance Raman scattering is studied.

1. Introduction

The amplification of spontaneous emission allows the generation of frequency tunable picosecond light pulses in dye solutions if population inversion is caused by excitation with picosecond pump sources[1-11]. Longitudinal[1,4,5,11], transversal[2,3,12], and travelling-wave transversal[6-10] pumping arrangements have been used. In transversally excited dye cells the duration of the amplified spontaneous emission signal is restricted by the transit time through the pumped region, and two pulses are emitted in opposite direction. The travelling-wave transverse pumping applies a grating for matching the propagation of the pump pulse to the amplified spontaneous emission signal. High gains are achieved in transverse and travelling-wave transverse pumping since excited-state absorption of the pump pulse has negligible influence on the transverse amplification of the fluorescence signal. In a longitudinally pumped dye cell the excited-state absorption at the pump-laser frequency ν_L restricts the amplification of the fluorescence light.

In this paper a versatile longitudinally pumped dye laser generator-amplifier system is described. The drawbacks of excited-state absorption at ν_L are avoided by splitting the pump pulse to pump a generator cell (amplification of spontaneous emission) and a chain of amplifier cells (signal amplification). The spectral narrowing and tuning is achieved with a grating spectrometer. The reamplification of the spectrally narrowed and tuned signals gives nearly bandwidth-limited intense picosecond light pulses.

2. Experimental

A schematic of the experimental setup is depicted in Fig.1. The pump pulses are generated in a passively mode-locked ruby laser (wavelength $\lambda_L = 694.3$ nm, duration $\Delta t_L \simeq 30$ ps). The generated ASE signal in the generator cell G is collimated (lens L2) and amplified in the longitudinally pumped dye cells A1 and A2. The spectrometer SP1 is used for spectral narrowing and tuning. The reamplification of the narrowed signal occurs in the dye cell A3 which is excited with an amplified fraction of the picosecond ruby pump pulse.

3. Dyes

The investigated dyes are listed in Table 1 together with some spectroscopic data. The absorption cross-sections σ_L at the pump laser frequency ν_L are measured with a spectrophotometer. The excited-state absorption cross-sections σ_{ex} are determined by intensity dependent transmission measurements[13]. The excited-state absorptions σ_{ex}^{ASE} of the generated light are determined by simulating the light generation in the generator cell[14]. The fluorescence lifetimes are measured with a streak camera at low dye concentrations. The fluorescence quantum efficiencies are measured with a spectro-fluorimeter[15]. The stimulated emission cross-section spectra are plotted in Fig.2. They are determined from absorption cross-section spectra and fluorescence quantum distribution measurements according to[16-19]

$$\sigma_{em}(\lambda) = \frac{n_F \lambda^4 \tilde{E}(\lambda) q_F}{n_A \tau_F} \frac{\int_{em} \tilde{E}(\lambda) d\lambda}{\int_{em} \tilde{E}(\lambda) \lambda^4 d\lambda} \int_{abs} \frac{\sigma_{abs}(\lambda)}{\lambda} d\lambda \qquad (1)$$

n_F and n_A are the average refractive indices of the solutions in the S_1-S_0 emission and the S_0-S_1 absorption band, respectively. $\tilde{E}(\lambda)$ is the normalized fluorescence quantum distribution ($\int_{em} \tilde{E}(\lambda) d\lambda = 1$).

4. Results

The amplification of spontaneous emission in the generator cell is studied first. Then the signal amplification, the spectral narrowing and tuning as well as the reamplification are investigated. The alternative technique of intense frequency tunable picosecond pulse

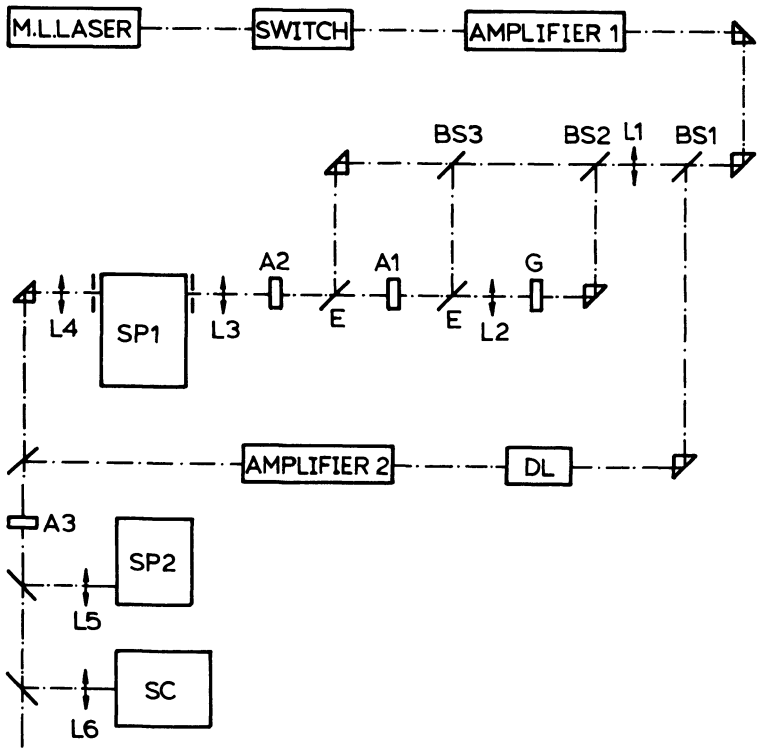

Fig.1: Experimental setup. L1-L6, lenses. G, generator dye cell. A1-A3, amplifier dye cells. SP1,SP2, grating spectrometers. DL, optical delay line. SC, streak camera. BS1-BS3, beam-splitters with reflectivities R1 = 0.1, R2 = 0.3, and R3 = 0.5. E, edge filters reflecting the pump pulse and transmitting the generated light.

generation by seeding pulse amplification of picosecond light continua is discussed shortly. The concurrent resonance Raman scattering is mentioned.

4.1 Amplified Spontaneous Emission in the Generator Cell. In the generator cell the fluorescence signal is amplified in forward direction. The dashed curves of Fig.3 display the normalized fluorescence spectral distributions $W_{FL}(\lambda)/W_L$ within an acceptance angle of $\Delta\Theta=6°$. The solid curves show the normalized spectral distribution $\eta_E(\lambda) = W_{ASE}(\lambda)/W_L$ of the amplified spontaneous emission (ASE) signals for $I_{0L} \approx 4\times10$ W/cm². W_L is the pump pulse energy at the entrance of the generator cell. The amplification and spectral narrowing of the fluorescence light are clearly seen. The ASE spectra are influenced by the applied dye concentrations. Higher dye concentrations shift the emission spectra to longer wavelengths because of fluorescence reabsorption (no curves shown). The wavelength-integrated ASE energy conversion efficiency W_{ASE}/W_L versus input pump pulse peak intensity is displayed in Fig.4 (circles and solid curve) for 10^{-4} molar DDI in methanol.

The amplification in forward direction reduces the divergence of the ASE signal. The divergence $\Delta\Theta$ versus I_{0L} is plotted in Fig.5 for 10^{-4} molar DDI in methanol (circles and curve 1).

The spectral bandwidth reduces with the pump pulse intensity (gain narrowing) and the emission peak shifts to shorter wavelengths (bleaching of reabsorption). This behaviour is shown in Fig.6 for 10^{-4} molar DDI in methanol. The spectral distribution of the generated spectrum is strongly structured when the observation angle is narrowed to the coherence angle $\Delta\Theta_{coh} = \lambda_{ASE}/d$ (d is approximately the beam diameter of the pump pulse). The statistical nature of the spontaneous emission and the coherent amplification are responsible for the fluctuating structure [20,21]. Integration over the full divergence angle results in a rather smooth spectrum [14].

The pulse duration of the ASE signal is shortened with rising pump pulse intensity. The circles and curve 1 of Fig.7 depict the dependence of the ASE pulse duration on the input pump pulse peak intensity for 2×10^{-3} molar rhodamine 800 in methanol. The dash-dotted curve represents the pump pulse duration. When the observation angle is narrowed to the coherence angle the temporal pulse shapes are structured. The pulse shapes are rather smooth when the ASE signal is integrated over the full divergence angle.

4.2 Amplifier Chain. The following results belong to the amplified ASE signal behind the second amplifier of Fig.1. The ASE signal behind the generator cell is collimated to improve the overlap between ASE signal and pump pulse cross-section.

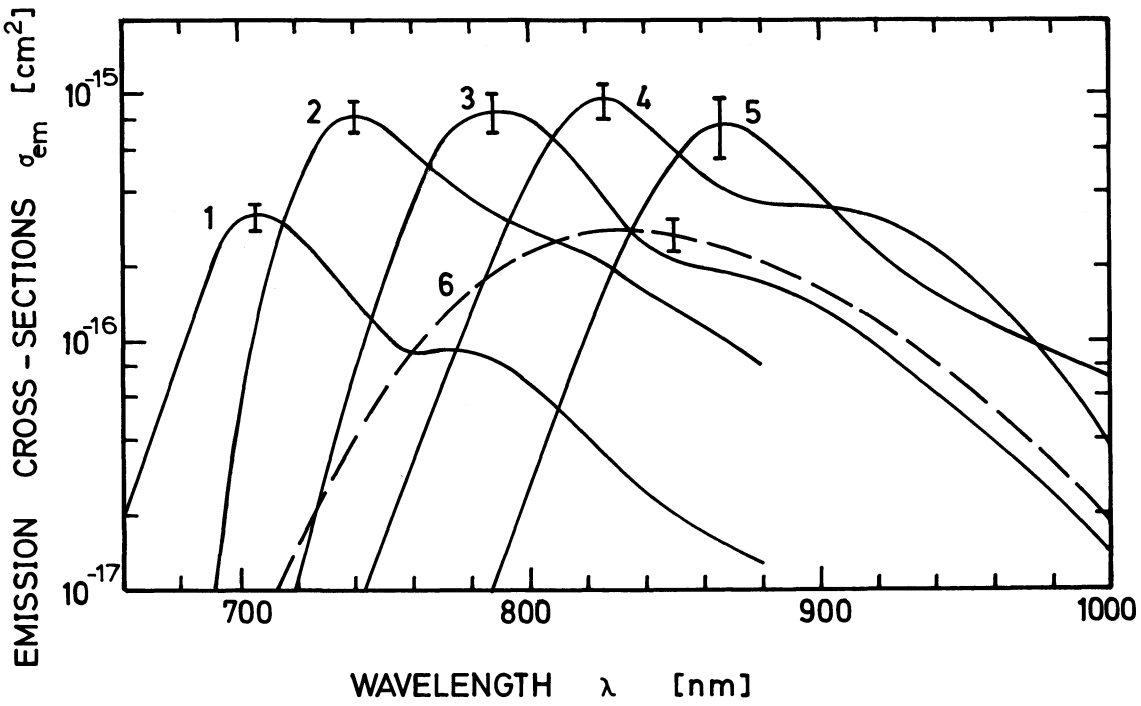

Fig.2: Stimulated emission cross-sections of investigated dyes. 1, rhodamine 800. 2, DDI. 3, HITCI. 4, HDITCI. 5, IR 140. 6, styril 9.

Table 1: Investigated dyes (all dyes supplied by Lambda Physik).
ME = methanol. EG/DMSO = 1:1 volume mixture of ethylene glycol and dimethyl sulfoxide.
DDI = 1,1'-diethyl-2,2'-dicarbocyanine iodide. HITCI = 1,1',3,3,3',3'-hexamethylindotricarbocyanine iodide. HDITCI = 1,1',3,3,3',3'-hexamethyl-4,4',5,5'-dibenzo-2,2'-indotricarbocyanine iodide.

Dye	Solvent	σ_L [cm²]	σ_{ex}^L [cm²]	σ_{ex}^{ASE} [cm²]	τ_F [ns]	q_F
DDI	ME	7.6×10^{-16}	5×10^{-17}	6×10^{-17}	0.017	0.004
Rhodamine 800	ME	2×10^{-16}	8×10^{-18}	1.3×10^{-17}	1.54	0.16
HITCI	ME	3.1×10^{-16}	8.5×10^{-17}	1.3×10^{-16}	0.46	0.12
HDITCI	EG/DMSO	2.2×10^{-16}	8.5×10^{-17}	1.1×10^{-16}	0.22	0.057
Styril 9	DMSO	3.9×10^{-17}	6×10^{-17}	$\sim 1.2\times10^{-16}$	0.39	0.05
IR 140	EG/DMSO	1.15×10^{-16}	1.15×10^{-16}	7×10^{-17}	0.24	0.047

The dash-dotted curves of Fig.3 show the normalized spectral distributions $W_{AMP}(\lambda)/W_L$ at $I_{OL} \approx 4\times10^9$ W/cm². The signal amplification versus pump pulse intensity (I_{OL} is intensity in front of generator cell) is indicated in Fig.4 (dots and dashed curve).

The divergence of the amplified signal is reduced drastically as is seen by the dots and the curve 2 in Fig.5 ($\Delta\Theta \approx d/\ell_{GA}$, d pump pulse diameter, ℓ_{GA} distance between generator cell and amplifier cell A2).

The spectral widths are slightly narrowed in the amplifier cells (Fig.3). The wavelength peak positions are practically unchanged. The spectral shapes are slightly smoothed due to gain saturation.

The duration of the amplified signals is shortened and becomes approximately equal to

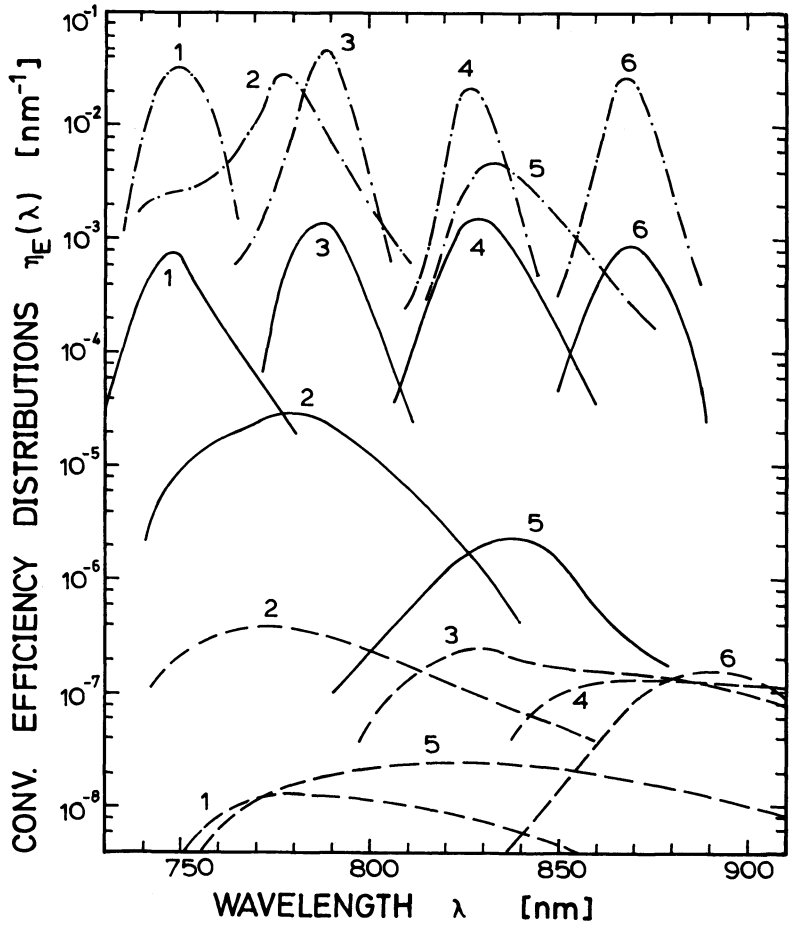

Fig.3: Conversion efficiency distributions. Dashed curves, fluorescence in forward direction within a divergence angle of $\Delta\Theta=6°$. Solid curves, amplified spontaneous emission signal after generator cell. Dash-dotted curves, signal behind second amplifier cell. 1, 10^{-4} molar DDI. 2, 2×10^{-3} molar rhodamine 800. 3, 7.7×10^{-5} molar HITCI. 4, 5.1×10^{-5} molar HDITCI. 5, 2.5×10^{-5} molar styril 9. 6, 3.7×10^{-5} molar IR 140. For solvents see Table 1. Length of dye cells is ℓ=1 cm.

the pump pulse duration as is seen by the triangle in Fig.7.

4.3 Tuning and Reamplification. The spectral width of the amplified ASE signal is typically 15 nm (Fig.3) and the duration is approximately 30 ps. The pulses are spectrally narrowed and tuned by passing through the spectrometer SP1. The spectral narrowing causes energy loss. The energy is restored by reamplification in the dye cell A3. The spectral narrowing, tuning, and reamplification are illustrated in Fig.8. The energy of the reamplified pulses is rather constant over a broad spectral range (higher gain at spectral wings since gain saturation occurs at the center spectral region).

4.4 Seeding Pulse Amplification. Besides the amplification of spontaneous emission the amplification of weak picosecond light continua [22] in dye cells may be applied to generate intense frequency tunable picosecond light pulses [11,14,23]. In Refs.11 and 14 the picosecond light continuum is generated in the ruby amplifier by focusing the selected single picosecond ruby pulse of the oscillator into the ruby amplifier. The main difference between amplified spontaneous emission and seeding pulse amplification (SPA) of a picosecond light continuum in a generator cell is the small divergence angle ($\Delta\Theta_{SPA} \simeq \Delta\Theta_L$, open triangles and curve 4 in Fig.5) and the short duration ($\Delta t_{SPA} < \Delta t_L$, open caro in Fig.7). Behind the amplifier cell A2 the beam divergence (filled triangles and curve 3 of Fig.5) is slightly enlarged and the pulse duration (filled caro in Fig.7) approaches the pump pulse duration.

4.5 Resonance Raman Scattering. The ASE signal behind the generator cell is free of Raman lines in all experiments. At the position of the pump pulse peak intensity where the Raman amplification is highest, the ASE signal is still too weak to show up as an amplified Raman signal. In the seeding pulse amplification of picosecond light continua, Stokes Raman lines of the dye molecules have been observed upon the amplified continuum at high pump pulse intensities in some dye solutions [11,14]. Behind the amplifier cells the same Raman lines were found upon the amplified ASE signals [11,14]. The Raman transitions are resonantly enhanced by the S_0-S_1 absorption of the pump laser [24].

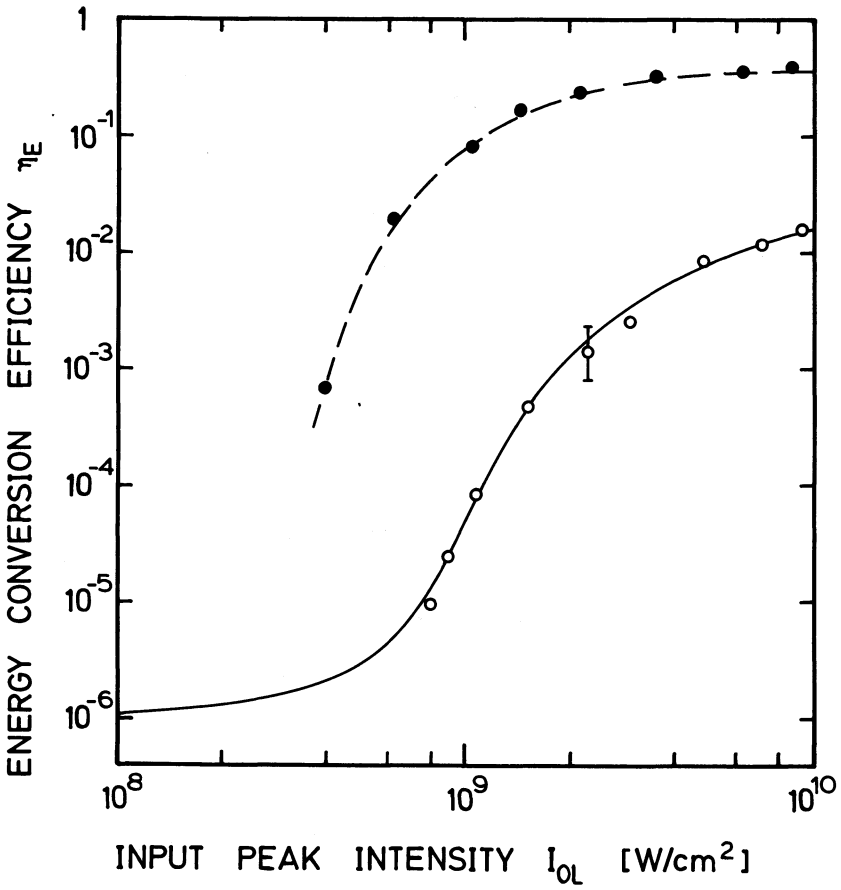

Fig.4: Energy conversion efficiency versus pump pulse peak intensity. Dye solution is 10^{-4} molar DDI in methanol. Circles and solid curve, ASE signal behind generator cell. Dots and dashed curve, amplified signal behind second amplifier cell. Cell lengths ℓ=1 cm.

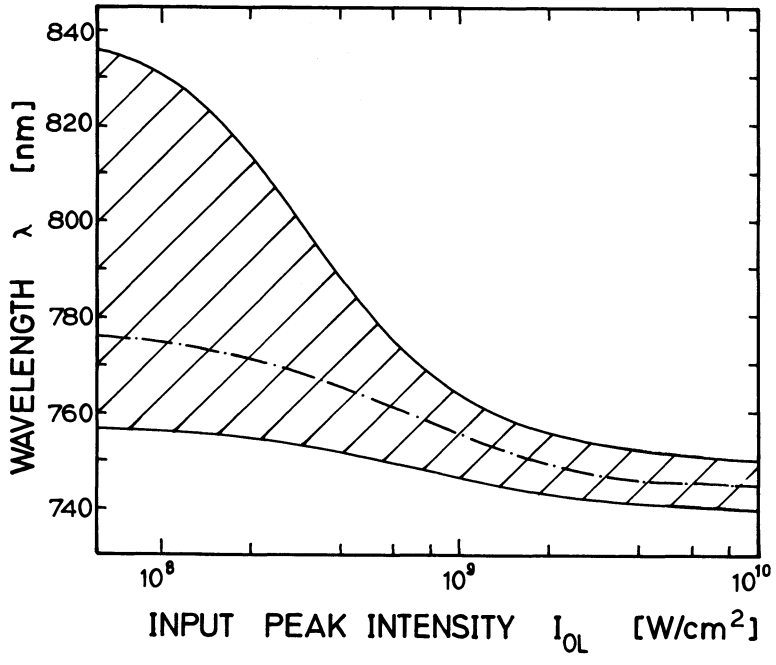

Fig.6: Wavelength of ASE emission versus pump pulse peak intensity for 10^{-4} molar DDI in methanol. Dash-dotted curve represents peak emission wavelength. The borders of the hatched region indicate the half-heights of the signal.

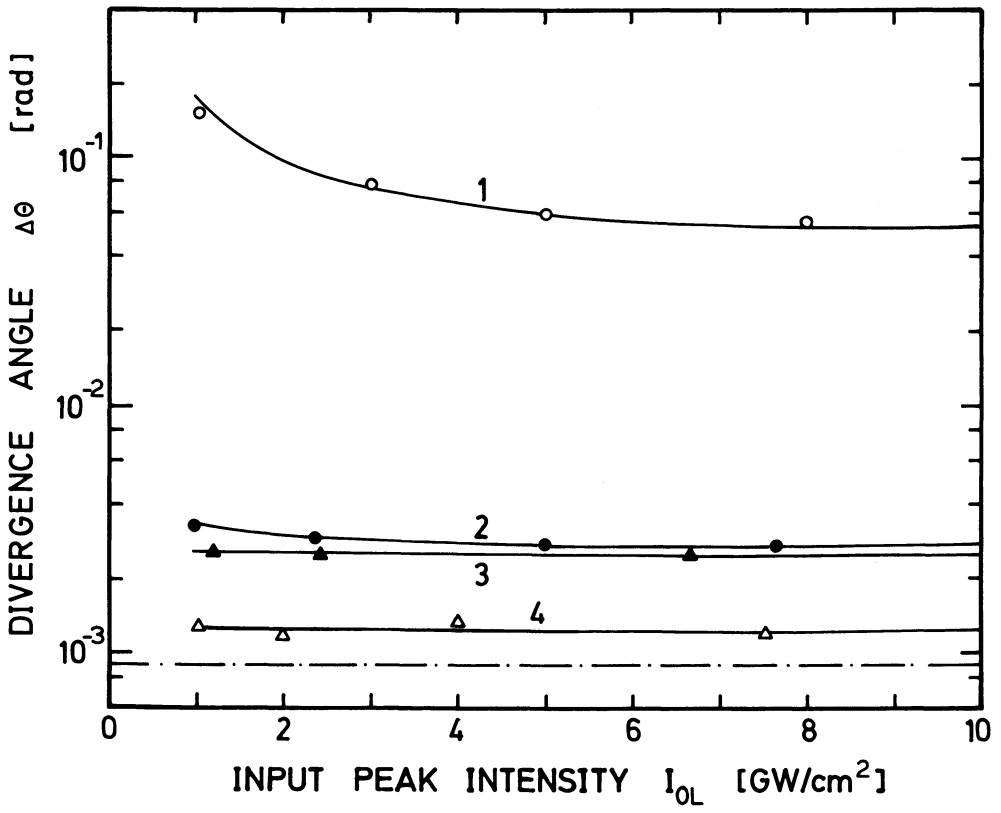

Fig.5: Beam divergence Δθ (FWHM) versus pump pulse peak intensity for 10^{-4} molar DDI in methanol. The curves belong to: (1,o), ASE signal behind generator cell G; (2,●), ASE signal behind amplifier cell A2; (3,▲), amplified picosecond light continuum behind amplifier cell A2; (4,Δ), amplified picosecond light continuum behind generator cell G. The dash-dotted curve represents the beam divergence of the pump pulse.

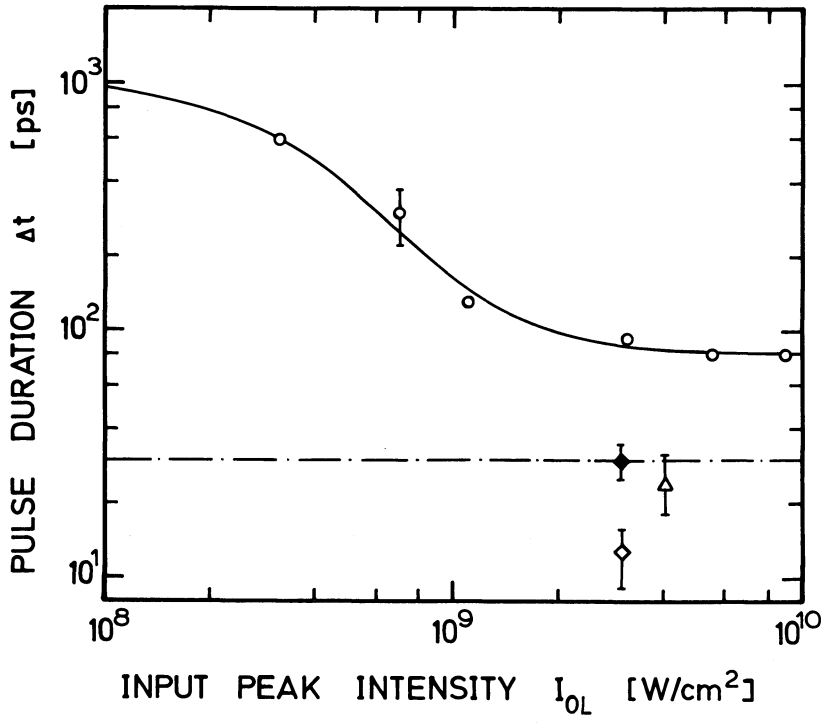

Fig.7: Pulse durations versus pump pulse peak intensity for 2×10^{-3} molar rhodamine 800 in methanol. Solid curve and circles, ASE signal behind generator cell. Triangle, ASE signal behind amplifier cell A2. Open caro, amplified picosecond light continuum behind generator cell G. Filled caro, amplified picosecond light continuum behind amplifier cell A2. Dash-dotted line, pump pulse duration Δt_L.

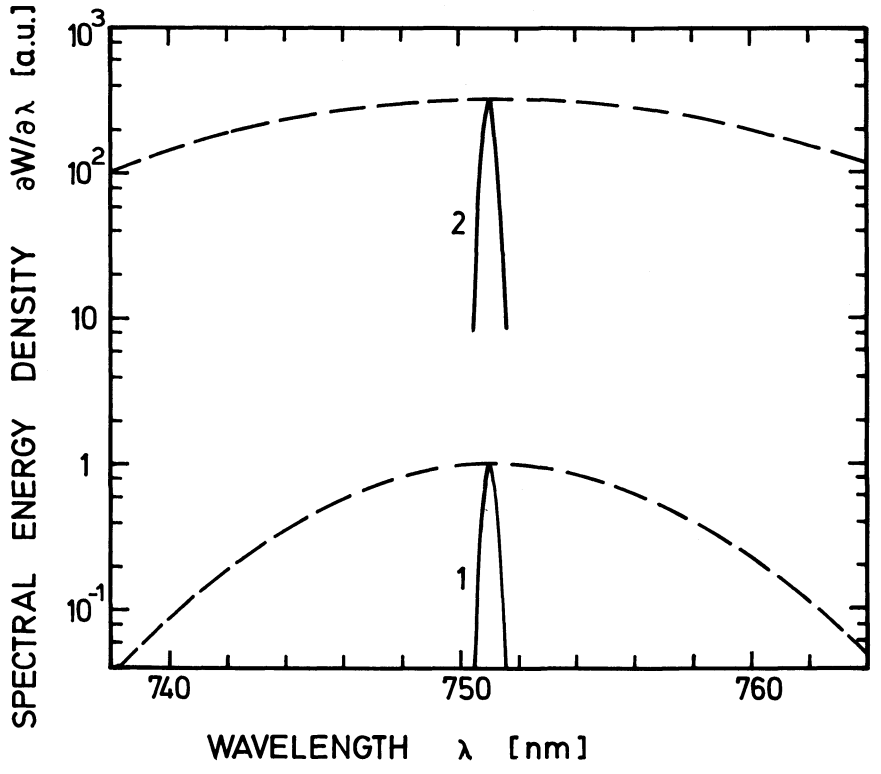

Fig.8: Reamplification of spectrally narrowed signal. Dye solution is 10^{-4} molar DDI in methanol. Solid curve 1, spectral distribution of amplified picosecond light continuum before amplifier A3. Solid curve 2, spectral distribution behind amplifier A3. The dashed curves are the envelopes of the peaks of the spectrally narrowed signals before and behind the amplifier A3.

5. Conclusions

The described dye generator-amplifier system allows the generation of intense, frequency tunable picosecond light pulses over a wide spectral range. With picosecond ruby pump pulses the frequency region between 720 nm and 940 nm was covered with 6 different dyes (in addition to Fig.3 5×10^{-4} molar rhodamine 800 extends the spectral range to 720 nm and 5×10^{-4} molar IR 140 extends the ASE signal to 940 nm). A conversion efficiency of approximately 10 % was obtained (relating to the pump pulse energy behind the ruby amplifier 1). Using other pump sources (second harmonic of mode-locked ruby laser, mode-locked Nd-lasers and their harmonics) the spectral region may be extended from the near ultraviolet to the near infrared spectral region over the full spectral range of available laser dyes or saturable absorbers[25-29]. In contrast to dye laser oscillators the picosecond dye laser generators may be operated as well with laser dyes of high fluorescence quantum efficiency and with saturable absorbers of low fluorescence quantum efficiency (short fluorescence lifetime τ_F, e.g. DDI in methanol)[6,9]. The generator efficiency is expected to reduce only if $\tau_F < \Delta t_L$.

References

1. M.E. Mack, Appl. Phys. Lett. 15, 166 (1969)
2. S.L. Chin and G. Bedard, Opt. Commun. 4, 148 (1971)
3. C. Lin, T.K. Gustafson, and A. Dienes, Opt. Commun. 8, 210 (1973)
4. A.N. Rubinov, M.C. Richardson, K. Sala, and A.J. Alcock, Appl. Phys. Lett. 27, 358 (1975)
5. W. Falkenstein, A. Penzkofer, and W. Kaiser, Opt. Commun. 27, 151 (1978)
6. H.J. Polland, T. Elsaesser, A. Seilmeier, and W. Kaiser, Appl. Phys. B32, 53 (1983)
7. Zs. Bor, S. Szatmari, and A. Müller, Appl. Phys. B32, 101 (1983)
8. S. Szatmari and F.P. Schäfer, Opt. Commun. 49, 281 (1984)
9. T. Elsaesser, H.J. Polland, A. Seilmeier, and W. Kaiser, IEEE J. QE-20, 191 (1984)
10. W. Lee, C. Ning, and Z. Huang, Appl. Phys. B40, 35 (1986)
11. P. Sperber, M. Weidner, and A. Penzkofer, Appl. Phys. B32, 185 (1987)
12. A. Penzkofer, Appl. Phys. B40, 85 (1986)
13. G. Grönninger and A. Penzkofer, Opt. Quantum Electron. 16, 225 (1984)

14. P. Sperber, W. Spangler, B. Meier, and A. Penzkofer, Opt. Quantum Electron., to be published
15. A. Penzkofer and W. Blau, Opt. Quantum Electron. 15, 325 (1983)
16. S.J. Strickler and R.A. Berg, J. Chem. Phys. 37, 814 (1962)
17. J.B. Birk and D.J. Dyson, Proc. Roy. Soc. London A275, 135 (1963)
18. O.G. Peterson, J.P. Webb, W.C. McColgin, and J.H. Eberly, J. Appl. Phys. 42, 1917 (1971)
19. A. Penzkofer and W. Leupacher, J. Luminesc. 37, 61 (1987)
20. A.A. Grütter, H.P. Weber, and R. Dändliker, Phys. Rev. 185, 629 (1969)
21. L. Mandel and E. Wolf, Rev. Mod. Phys. 37, 231 (1965)
22. A. Penzkofer and W. Kaiser, Opt. Quantum Electron. 9, 315 (1977)
23. A. Migus, J.L. Martin, R. Astier, A. Antonetti, and A. Orizag, in Picosecond Phenomena III, K.B. Eisenthal, R.M. Hochstrasser, W. Kaiser, and A. Laubereau (Springer-Verlag, Berlin, 1982) p. 6
24. M. Pfeiffer, A. Lau, and W. Werncke, J. Raman Spectrosc. 15, 20 (1984)
25. F.P. Schäfer, Editor, Dye Lasers (Springer-Verlag, Berlin 1977)
26. M. Maeda, Laser Dyes (Academic Press, New York, 1984)
27. U. Brackmann, Laser-grade Dyes (Lambda Physik, Göttingen, 1986)
28. Kodak Laser Dyes (Kodak Publication JJ-169, 1987)
29. H.J. Polland, T. Elsaesser, A. Seilmeier, W. Kaiser, M. Kussler, N.J. Marx, B. Sens, and K.H. Drexhage, Appl. Phys. B32, 53 (1983)